DMD Fast Forward. Published on October 29, 2024 as DOI: 10.1124/dmd.124.001917
This article has not been copyedited and formatted. The final version may differ from this version.

Characterization of human alcohol dehydrogenase 4 and aldehyde dehydrogenase 2 as enzymes involved in the formation of 5-carboxylpirfenidone, a major metabolite of pirfenidone

Rei Sato, Tatsuki Fukami, Kazuya Shimomura, Yongjie Zhang, Masataka Nakano, and Miki Nakajima

Drug Metabolism and Toxicology, Faculty of Pharmaceutical Sciences, Kanazawa University, Kakuma-machi, Kanazawa, Japan (R.S., T.F., K.S., M.N., and M.N.); WPI Nano Life Science Institute (WPI-NanoLSI), Kanazawa University, Kakuma-machi, Kanazawa, Japan (T.F., Y.Z., M N., and M.N.); and Clinical Pharmacokinetics Laboratory, School of Basic Medicine and Clinical Pharmacy, China Pharmaceutical University, Nanjing, China (Y.Z.)

Running title

ADH4 and ALDH2 catalyze 5-hydroxylpirfenidone oxidation

Correspondence

Tatsuki Fukami, Ph.D.

Drug Metabolism and Toxicology, Faculty of Pharmaceutical Science; WPI Nano Life Science Institute (WPI-NanoLSI), Kanazawa University

Kakuma-machi, Kanazawa 920-1192, Japan

Tel: +81-76-234-4438 / Fax: +81-76-264-6282

E-mail: tatsuki@p.kanazawa-u.ac.jp

Number of text pages: 34

Number of tables: 3

Number of figures: 8

Number of references: 37

Number of words in Abstract: 241 words

Number of words in Introduction: 422 words

Number of words in Discussion: 1399 words

Abbreviations

ADH, alcohol dehydrogenase; ALDH, aldehyde dehydrogenase; 5-COOH PIR, 5-carboxylpirfenidone, CYP, cytochrome P450; DMSO, dimethyl sulfoxide; HLC, human liver cytosol; HLM, human liver microsomes; 5-OH PIR, 5-hydroxylpirfenidone, PIR, pirfenidone; 5-CHO PIR, pirfenidone aldehyde; SEM, semicarbazide

DMD Fast Forward. Published on October 29, 2024 as DOI: 10.1124/dmd.124.001917
This article has not been copyedited and formatted. The final version may differ from this version.

Abstract

Pirfenidone (PIR) is used to treatment of idiopathic pulmonary fibrosis. After oral administration, it is metabolized by cytochrome P450 1A2 to 5-hydroxylpirfenidone (5-OH PIR) and further oxidized to 5-carboxylpirfenidone (5-COOH PIR), a major metabolite excreted in the urine (90% of the dose). This study aimed to identify enzymes that catalyze the formation of 5-COOH PIR from 5-OH PIR in the human liver. 5-COOH PIR was formed from 5-OH PIR in the presence of NAD^+ by human liver microsomes (HLM) more than by human liver cytosol (HLC), with the concomitant formation of the aldehyde form (5-CHO PIR) as an intermediate metabolite. By purifying enzymes from HLM, alcohol dehydrogenases (ADHs) were identified as candidate enzymes catalyzing 5-CHO PIR formation, although ADHs are localized in the cytoplasm. Among constructed recombinant ADH1–5 expressed in HEK293T cells, only ADH4 efficiently catalyzed 5-CHO PIR formation from 5-OH PIR with a K_m value (29.0 ± 4.9 μM), which was close to that by HLM (59.1 ± 4.6 μM). In contrast to commercially available HLC, in-house prepared HLC clearly showed substantial 5-CHO PIR formation, and ADH4 protein levels were significantly (rs = 0.772, $P < 0.0001$) correlated with 5-CHO PIR formation in 25 in-house prepared HLC samples. Some components of the commercially available HLC may inhibit ADH4 activity. Disulfiram, an inhibitor of aldehyde dehydrogenases (ALDH), decreased 5-COOH PIR formation and increased 5-CHO PIR formation from 5-OH PIR in HLM. ALDH2 knockdown in HepG2 cells by siRNA decreased 5-COOH PIR formation by 61%.

DMD Fast Forward. Published on October 29, 2024 as DOI: 10.1124/dmd.124.001917
This article has not been copyedited and formatted. The final version may differ from this version.

Significance statement

This study clarified that 5-COOH PIR formation from 5-OH PIR proceeds via a two-step oxidation reaction catalyzed by ADH4 and disulfiram-sensitive enzymes, including ALDH2. Inter-individual differences in the expression levels or functions of these enzymes could cause variations in the pharmacokinetics of PIR.

DMD Fast Forward. Published on October 29, 2024 as DOI: 10.1124/dmd.124.001917
This article has not been copyedited and formatted. The final version may differ from this version.

Introduction

Pirfenidone (PIR), which can inhibit the production of transforming growth factor-β and the release of tumor necrosis factor-α from macrophages (Hirano et al., 2006), is used as a first-line drug for the treatment of idiopathic pulmonary fibrosis (Richeldi et al., 2017). After oral administration, PIR is rapidly absorbed from the intestine and metabolized only in the liver to 5-hydroxylpirfenidone (5-OH PIR) and then to 5-carboxylpirfenidone (5-COOH PIR), which is excreted in the urine at approximately 90% of the dose (Huang et al., 2013) (Fig. 1). As these metabolites appear to be pharmacologically inactive (https://www.accessdata.fda.gov/drugsatfda_docs/label/2014/ 022535s000lbl.pdf), the variability in the metabolic clearance of PIR to 5-COOH PIR is a key determinant of the variable efficacy of PIR. Previously, we reported that the formation of 5-OH PIR from PIR in the human liver is primarily catalyzed by cytochrome P450 (P450, CYP) 1A2 and partially by CYP2C19 and CYP2D6 (Zhang et al., 2021) (Fig. 1). However, the enzymes that catalyze the formation of 5-COOH PIR from 5-OH PIR have not yet been identified, although 5-COOH PIR is a major metabolite of PIR (Huang et al., 2013). Since alcohols are generally oxidized to their corresponding carboxylic acids via the formation of aldehydes (Di et al., 2021), an aldehyde is expected to form as an intermediate metabolite.

It is widely accepted that the oxidation of alcohol to the corresponding aldehyde is catalyzed by alcohol dehydrogenase (ADH) or cytochrome P450 isoforms using β-NAD^+ and β-NAPDH as cofactors, respectively (Di et al., 2021; Zanger and Schwab, 2013). The human ADH family consists of seven isoforms (ADH1A, ADH1B, ADH1C, ADH4, ADH5, ADH6, and ADH7), the first five of which are expressed in the liver (Di et al., 2021). Aldehyde dehydrogenase (ALDH), aldehyde oxidase (AOX), and xanthine oxidase (XO) catalyze the oxidation of aldehydes to their corresponding carboxylic acids (Di et al., 2021; Fukami et al., 2022). The human ALDH family consists of 19 isoforms, and eleven isoforms (ALDH1A1,

DMD Fast Forward. Published on October 29, 2024 as DOI: 10.1124/dmd.124.001917
This article has not been copyedited and formatted. The final version may differ from this version.

ALDH1A2, ALDH1B1, ALDH1L1, ALDH2, ALDH3A2, ALDH4A1, ALDH5A1, ALDH6A1, ALDH8A1, and ALDH9A1) are expressed in the liver (Ma et al., 2011). AOX, the sole functional enzyme in its family, and XO, the enzyme that do not form a family, are also expressed in the human liver (Terao et al., 2016; Harrison, 2002).

The identification of enzymes responsible for drug metabolism would provide clues for predicting inter- or intra-individual variability in drug efficacy. To clarify the metabolism of PIR at the molecular level, this study aimed to identify the enzymes involved in the formation of 5-COOH PIR from 5-OH PIR in the human liver.

DMD Fast Forward. Published on October 29, 2024 as DOI: 10.1124/dmd.124.001917
This article has not been copyedited and formatted. The final version may differ from this version.

Materials and methods

Materials. PIR, 5-OH PIR, and 5-COOH PIR were obtained from Shionogi Pharmaceutical (Osaka, Japan). β-$NADP^+$, β-NADPH, β-NAD^+, and β-NADH were obtained from Oriental Yeast (Tokyo, Japan). Disulfiram, phthalazine, phthalazone, and semicarbazide (SEM) were purchased from FUJIFILM Wako Pure Chemicals (Osaka, Japan). Human liver microsomes (HLM) (pooled, n = 50) and human liver cytosols (HLC) (pooled, n = 150) were purchased from Corning (Corning, NY). Mouse anti-human ADH, ADH5, and ALDH1A1 monoclonal antibodies were purchased from Santa Cruz Biotechnology (Santa Cruz, CA). Rabbit anti-human ADH4 and ALDH2 polyclonal antibodies were obtained from Proteintech (Tokyo, Japan) and ABclonal (Boston, MA), respectively. IRDye680 goat anti-mouse antibody was obtained from LI-COR Biosciences (Lincoln, NE). Lipofectamine 3000 (Invitrogen), Silencer Select siRNAs for human ALDH1A1 (siALDH1A1), human ALDH2 (siALDH2), and negative control #1 (siControl) were purchased from Thermo Fisher Scientific (Waltham, MA). All other chemicals and solvents were of the highest commercially available quality.

Cell culture. Human embryonic kidney-derived HEK293T cells and human hepatoma-derived HepG2 cells purchased from the American Type Culture Collection (ATCC; Manassas, VA) and RIKEN (Tsukuba, Japan), respectively, were cultured in Dulbecco's modified Eagle's medium (DMEM) containing 10% fetal bovine serum (FBS; Invitrogen, Carlsbad, CA) in a 5% CO_2 atmosphere at 37 °C. The medium used to culture HepG2 cells also contained 0.1 mM non-essential amino acids (Invitrogen).

Construction of recombinant ADH and ALDH isoforms expressed in HEK293T cells. cDNA was synthesized from total RNA prepared from a human liver sample using ReverTra Ace according to the manufacturer's protocol. ADH1A, ADH1B, ADH1C, ADH4, and ADH5 cDNAs were obtained using polymerase chain reaction (PCR) with the primers listed in Table 1. PCR products were subcloned into the pTargeT mammalian expression vector (Promega,

Madison, WI). Nucleotide sequences were confirmed by sequence analysis (FASMAC, Kanagawa, Japan) to be identical to the reference sequences (ADH1A: NM_000667.4; ADH1B: NM_000668.6; ADH1C: MN_000669.5; ADH4: NM_000670.5; and ADH5: NM_000671.4). Plasmids containing ADH1A, ADH1B, ADH1C, ADH4, or ADH5 cDNA were transfected into HEK293T cells on collagen-coated 10 cm-dishes. After 24 h, 2 μg of plasmid was transfected into the cells using Lipofectamine 3000. After 48 h, the cells were harvested, and cell homogenates were prepared as recombinant ADH1A, ADH1B, ADH1C, ADH4, and ADH5. The protein concentrations were determined by the method of Bradford (Bradford, 1976) using γ-globulin as the standard.

Preparation of microsomal and cytosolic fractions from individual human liver samples. Human liver samples from 27 donors (Supplemental Table 1) were obtained from the Human and Animal Bridging Research Organization (Chiba, Japan) in partnership with the National Disease Research Interchange (Philadelphia, Philadelphia). The use of human livers was approved by the Ethics Committee of Kanazawa University (Kanazawa, Japan). Microsomal and cytosolic fractions were prepared as described previously (Kobayashi et al., 2012). The protein concentrations were determined as described above (Bradford, 1976).

Measurement of the formation of 5-COOH PIR from 5-OH PIR by HLM or HLC. The formation of 5-COOH PIR from 5-OH PIR was evaluated as follows: a typical incubation mixture (final volume of 200 μL) contained 100 mM Tris-HCl buffer (pH 8.5), 0.5 mg/mL HLM or HLC, and 50 μM 5-OH PIR dissolved in dimethyl sulfoxide (DMSO). The final concentration of DMSO was 1%. In the inhibition study, disulfiram, an inhibitor of ALDH (Tomlinson et al., 1997), was added to the reaction mixture at a concentration of 20 μM (final concentration of DMSO was 2%). After pre-incubation at 37 °C for 3 min, the reaction was initiated by adding NAD^+, NADH, $NADP^+$, or NADPH at a final concentration of 1 mM. After incubation at 37 °C for 30 min, the reaction was terminated by adding 200 μL ice-cold 2% perchloric acid (PCA). The mixture was centrifuged at 13,000g for 20 min, and 50 μL of

the supernatant was subjected to high-performance liquid chromatography (HPLC). The HPLC system consisted of a Chromaster 5210 autosampler (Hitachi, Tokyo, Japan), Chromaster 5110 pump (Hitachi), Chromaster 5310 column oven (Hitachi), and Chromaster 5420 UV-VIS detector (Hitachi). Wakopack eco-ODS column (4.6 × 150 mm, 3 μm; FUJIFILM Wako Pure Chemical) was used, and the column temperature was set at 40 °C. The mobile phases consisted of (A) 0.2% formic acid containing 0.8% acetonitrile and (B) acetonitrile containing 0.2% formic acid. The elution conditions were as follows: 10% B (0–5 min), 10–70% B (5–15 min), 70–95% B (15–15.5 min), 95% B (15.5–18.5 min), 95–10% B (18.5–19 min), and 10% B (19–25 min). The flow rate was 1 mL/min and the eluent was monitored at 310 nm. Quantification of the 5-COOH PIR was performed by comparing the HPLC peak area with that of the authentic standard.

Detection of pirfenidone aldehyde (5-CHO PIR) from 5-OH PIR by HLM. To investigate whether 5-CHO PIR was formed from 5-OH PIR, liquid chromatography-tandem mass spectrometry (LC-MS/MS) analysis was performed as follows: 10 μL of the reaction mixture as described previously was injected into an LC-20AD HPLC system equipped with LCMS-8045 (Shimadzu, Kyoto, Japan). Develosil ODS-UG-3 (2.0 × 150 mm, 3 μM; Nomura Chemical, Seto, Japan) was used, and the column temperature was set at 40°C. The mobile phases consisted of (A) 0.1% formic acid and (B) acetonitrile containing 0.1% formic acid. The elution conditions were as follows: 20% B (0.01–2 min), 20–50% B (2–8 min), 50% B (8–12 min), 50–20% B (12–13 min), and 20% (13–15 min). The flow rate was 0.2 mL/min. Nitrogen was used as the nebulizer and drying gas. The operating parameters were optimized as follows: nebulizer gas flow, 3 L/min; drying gas flow, 15 L/min; desolvation line temperature, 300 °C; and heat block temperature, 400 °C. LC-MS/MS was performed in positive electrospray ionization mode. A precursor ion scan from *m/z* 180 to 240 and single ion monitoring (SIM) at *m/z* 200.1 were performed to monitor 5-CHO PIR. With the *m/z* value set to 200.1 as the precursor ion, a product-ion scan was performed from *m/z* 30 to 180. Simultaneously, 5-COOH PIR was monitored by SIM at *m/z* 216.1, and a product ion scan

was performed at *m/z* 216.1 set as the precursor ion.

HPLC or LC-MS/MS analysis to detect a SEM conjugate formed by HLM, HLC, or recombinant ADHs. The formation of an SEM conjugate of 5-CHO PIR was determined. SEM was added to the reaction mixture described previously at a final concentration of 10 mM. The assay conditions were identical to those described previously. After centrifugation, the supernatant was subjected to HPLC to evaluate the peak area, which was considered to be an SEM conjugate. To verify that the peak obtained in the presence of SEM was the SEM conjugate of 5-CHO PIR, 10 μL of the supernatant was subjected to LC-MS/MS as described previously. The precursor ions were scanned from *m/z* 230 to 280. The precursor ion was set to *m/z* 257.2, and a product ion scan was performed from *m/z* 90–210.

Purification of enzymes catalyzing the formation of 5-CHO PIR from 5-OH PIR in HLM. To purify the enzymes that catalyze the formation of 5-CHO PIR from 5-OH PIR, HLM sample was solubilized in 100 mM potassium phosphate buffer (pH 7.4) containing 20% glycerol, 1 mM ethylenediaminetetraacetic acid (EDTA), and 0.3% sodium cholate at 4 °C for 8 h. After centrifugation at 105,000g at 4 °C for 1 h, 50–70% of ammonium sulfate was added and centrifuged at 10,000g at 4 °C for 30 min. The pellets were resuspended in buffer A (100 mM Tris-HCl buffer [pH 8.5] containing 20% glycerol, 1 mM EDTA, and 0.3% sodium cholate). The fraction was then dialyzed against buffer A to remove ammonium sulfate. The dialyzed sample was applied to a DEAE Sepharose anion exchange column (1.25 × 10 cm; GE Healthcare, Buckinghamshire, UK) equilibrated with buffer A. Proteins were eluted with buffer A containing 0–1 M KCl in a gradient mode at a rate of 0.5 mL/min. The eluate was sequentially collected as 1-mL aliquots, and their protein concentrations were determined as described previously. Formation of the SEM conjugate by the collected fractions was evaluated using HPLC, as described previously. Fractions showing a peak corresponding to the SEM conjugate (fractions 11–43) were pooled and centrifuged at 4,000 ×g using an Amicon Ultra-4 10 K concentrator (Millipore) to concentrate the proteins and

replace the buffer. The concentrated proteins were diluted with buffer B [20 mM Tris-HCl buffer (pH 9.0) containing 20% glycerol, 1 mM EDTA, and 0.3% sodium cholate] and applied to a DEAE Sephacel anion exchange column (1.25 × 10 cm; GE Healthcare) equilibrated with buffer B. Proteins were eluted with buffer B containing 0–1 M KCl in a gradient mode at a rate of 0.5 mL/min, and the formation of the SEM conjugate by each 1-mL fraction was evaluated. Fractions showing a peak corresponding to the SEM conjugate (fractions 6–20) were pooled and concentrated using an Amicon Ultra-4 10 K concentrator. The concentrated proteins were diluted in buffer C [10 mM potassium phosphate buffer (pH 8.0) containing 20% glycerol, 1 mM EDTA, and 0.3% sodium cholate] and then applied to a hydroxyapatite column (1.5 × 10 cm; Bio-Rad, Hercules, CA) equilibrated with buffer C. Proteins were eluted with buffer C containing 10–300 mM potassium phosphate in a gradient mode at a rate of 0.5 mL/min, and the SEM conjugate formation of each 1-mL fraction was evaluated. Fifteen microliters of the eluted fractions were subjected to sodium dodecyl-sulfate polyacrylamide gel electrophoresis (SDS-PAGE), followed by silver staining. The fractions showing a peak corresponding to the SEM conjugate (fractions 63–71) were pooled and centrifuged at 4,000 × g using an Amicon Ultra-4 10 K concentrator. Proteins in the final fraction were analyzed using a MALDI TOF/TOF 4800 Plus (AB Sciex, Toronto, Canada) at the Institute for Gene Research at Kanazawa University (Kanazawa, Japan).

SDS-PAGE, silver staining, and Western blotting. SDS-PAGE was performed as described previously (Ogiso et al., 2021). One microgram of HLM or fractions obtained from protein purification was separated on a 7.5% polyacrylamide gel. After electrophoresis, the gels were stained using a silver staining kit (Cosmo Bio, Tokyo, Japan), according to the manufacturer's instructions. For Western blotting, HLM or HLC (3 μg), recombinant ADH1A, ADH1B, ADH1C, ADH4, or ADH5 (3 μg) were separated on a 7.5% polyacrylamide gel and electrotransferred onto a polyvinylidene difluoride (PVDF) membranes (Immobilon-P; Millipore Corporation, Burlington, MA). The membrane was probed with a mouse anti-human ADH primary antibody, rabbit anti-human ADH4 primary antibody, mouse anti-human

DMD Fast Forward. Published on October 29, 2024 as DOI: 10.1124/dmd.124.001917
This article has not been copyedited and formatted. The final version may differ from this version.

ADH5 primary antibody, and the corresponding fluorescent dye-conjugated secondary antibody. ALDH1A1 and ALDH2 protein levels were determined using homogenate from HepG2 cells transfected with siRNA (40 μg) as described previously, and the membrane was probed with mouse anti-ALDH1A1 or rabbit ALDH2 primary antibodies and corresponding fluorescence dye-conjugated secondary antibodies. The bands were detected using an Odyssey Infrared Imaging system (LI-COR Biosciences).

Kinetic analysis of SEM conjugate formation from 5-OH PIR by HLM, HLC, or recombinant ADH4. SEM conjugate formation from 5-OH PIR by HLM, HLC, or recombinant ADH4 was measured at substrate concentrations of 5–600 μM in the presence of 20 μM disulfiram to inhibit the formation of 5-COOH PIR from 5-CHO PIR. Kinetic parameters were estimated from a Michaelis-Menten fitted curve using a computer program designed for nonlinear regression analysis (GraphPad Prism 5 software, San Diego, CA).

Correlation analysis between activity and untargeted proteomics data in HLC. The formation of SEM conjugate from 5-OH PIR by 25 individual HLC samples (Supplemental Table 1) was measured at a substrate concentration of 50 μM in the presence of 20 μM disulfiram to inhibit the formation of 5-COOH PIR from 5-CHO PIR. LC-MS/MS-based untargeted proteomics was previously conducted to comprehensively evaluate the relative expression levels of all proteins in 25 individual HLC samples (Kudo et al., 2023).

Transfection of siRNA into HepG2 cells and *in cellulo* assay for 5-COOH PIR formation. HepG2 cells were seeded and transfected with 5 nM siALDH1A1, siALDH2, or siControl, using Lipofectamine RNAiMAX (Thermo Fisher Scientific). After 72 h, the cells were treated with 50 μM 5-OH PIR. After 12 h, the amount of 5-COOH PIR in the medium was measured using HPLC as described previously.

Phthalazine oxidase activity. Phthalazine oxidase activity was measured by quantifying

DMD Fast Forward. Published on October 29, 2024 as DOI: 10.1124/dmd.124.001917
This article has not been copyedited and formatted. The final version may differ from this version.

phthalazone using HPLC according to a previously reported method (Amano et al., 2018), with slight modifications. Briefly, a typical incubation mixture (final volume of 200 μL) contained 25 mM potassium phosphate buffer (pH 7.4), 0.1 mM EDTA, and 0.5 mg/mL HLC or HLM, and the column used was Wakopack eco-ODS column (4.6 × 150 mm, 3 μm; FUJIFILM Wako Pure Chemical).

Statistical analysis. Statistical analyses were performed using one-way analysis of variance (ANOVA) and Tukey's tests. Correlation analyses were performed using the Spearman's rank method. Statistical significance was set at $P < 0.05$.

DMD Fast Forward. Published on October 29, 2024 as DOI: 10.1124/dmd.124.001917
This article has not been copyedited and formatted. The final version may differ from this version.

Results

5-COOH PIR formation from 5-OH PIR by HLM or HLC

Using commercially available pooled HLM (pHLM) or pooled HLC (pHLC), the formation of 5-COOH PIR from 5-OH PIR was measured at 50 μM substrate concentration (Fig. 2). The 5-COOH PIR was substantially formed in the presence of NAD^+ in pHLM (209.3 ± 29.9 pmol/min/mg) and was moderately formed in pHLC (54.6 ± 1.7 pmol/min/mg) (Fig. 2A), suggesting that the NAD^+-dependent enzyme(s) localized in endoplasmic reticulum rather than cytosol are primarily involved in the formation of 5-COOH PIR. In addition to the 5-COOH PIR peak, another peak (M1) was detected in HLM (Fig. 2B) in an incubation time- and protein-concentration-dependent manner (data not shown). Metabolite M1 was assumed to be an aldehyde form of 5-CHO PIR because an aldehyde metabolite is formed as an intermediate in the oxidation of an alcohol to the corresponding carboxylic acid (Di et al., 2021). To examine whether M1 corresponds to the 5-CHO PIR, the effects of disulfiram, an inhibitor of ALDHs that catalyze the oxidation of aldehydes to carboxylic acids, on M1 formation were examined. Because the addition of disulfiram increased M1 formation and abolished the 5-COOH PIR peak (Fig. 2B), M1 was suggested to be a 5-CHO PIR. In the Q1 scan at *m/z* 180–240, the pHLM sample incubated with 5-OH PIR and NAD^+ exhibited two peaks at *m/z* 216.1 and 200.1 (peaks 1 and 2, respectively) (Fig. 2C). By SIM at *m/z* 216.1 or 200.1, a single peak was clearly detected, with the same retention time as that of the Q1 scan (Fig. 2D). The elution order of 5-COOH and 5-CHO PIR (M1) determined by LC-MS/MS (Fig. 2D) was consistent with that determined using HPLC (Fig. 2B). Since the exact mass values of 5-COOH PIR and 5-CHO PIR are 215.1 and 199.1, respectively, the peaks at *m/z* 216.1 and 200.1 correspond to 5-COOH PIR and 5-CHO PIR, respectively. In the product ion scan, a daughter ion (*m/z* 77.0 was detected from both parent ions at 216.1 or 200.1, indicating that M1 is a 5-CHO PIR (Fig. 2E). These results suggest that the formation of 5-COOH PIR from 5-OH PIR proceeds in two steps: the formation of 5-CHO PIR from 5-OH PIR, and the subsequent formation of 5-COOH PIR from 5-CHO PIR.

DMD Fast Forward. Published on October 29, 2024 as DOI: 10.1124/dmd.124.001917
This article has not been copyedited and formatted. The final version may differ from this version.

Detection of 5-CHO PIR as an SEM conjugate

Because aldehydes are generally unstable (O'Brien et al., 2005), we sought to detect the 5-CHO PIR as a conjugate using SEM, which is widely used as a trapping reagent for aldehyde compounds (Inoue et al., 2015). Disulfiram, an ALDH inhibitor, was also added to the incubation mixture to inhibit the formation of 5-COOH PIR from 5-CHO PIR, because ALDH was assumed to catalyze this reaction. As shown in Fig. 3A, the addition of SEM resulted in the appearance of a new peak, M2, with a decreased peak of 5-CHO PIR in the HPLC analysis, suggesting that M2 would be an SEM conjugate of 5-CHO PIR. Using the Q1 scan of the LC-MS/MS analysis at *m/z* 230–280, the pHLM sample incubated with 5-OH PIR and SEM revealed a new peak (peak 3) with *m/z* value of 257.2 at a retention time earlier than that of 5-CHO PIR (Fig. 3B). Using SIM at *m/z* 257.2, a single peak was clearly detected at the same retention time as that of peak 3 in the Q1 scan (Fig. 3C). Because the predicted exact mass of the SEM conjugate of 5-CHO PIR was 256.3, the peak was judged to be the SEM conjugate. The product ion scan of the peak, of which precursor ion is *m/z* 257.2, showed signals at *m/z* 155.7 ($C_{10}H_8N_2$), 128.0 ($C_9H_7N_4$), and 171.2 ($C_{10}H_9N_3$), which correspond to the fragmentation pattern of the SEM conjugate of 5-CHO PIR (Fig. 3D). In subsequent experiments, 5-CHO PIR formation was evaluated by detecting the SEM conjugate using HPLC.

Purification of enzyme(s) catalyzing 5-CHO PIR formation from 5-OH PIR

To identify the enzymes responsible for 5-CHO PIR formation in HLM, proteins were isolated from HLM by monitoring SEM conjugate formation. The fractions obtained from a series of purification steps (ammonium sulfate precipitation, DEAE Sepharose, and hydroxyapatite chromatography) were separated by SDS-PAGE, followed by silver staining (Fig. 4A). Although multiple bands were obtained even in the fraction from the last purification step (lane 5), the band intensities of proteins with molecular weights of

approximately 25 and 40 kDa increased as the purification steps progressed, up to 9- and 46-fold higher than those in the initially solubilized HLM (lane 1), respectively (Fig. 4B). The SEM conjugate formation by the final fraction ($6.66 \pm 0.26 \times 10^6$ area/min/mg) was 55-fold higher than that by HLM ($0.12 \pm 0.01 \times 10^6$ area/min/mg) (Fig. 4B). Proteomic analysis of the fraction obtained in the final step revealed the presence of approximately 270 proteins. The top four proteins with a high SEQUEST HT score, the sum of scores of the individual peptides from the SEQUEST HT search (Thermo Fisher Scientific), were ADH isoforms ADH4, ADH1B, ADH1C, and ADH1A (Fig. 4C), suggesting that the protein catalyzing 5-CHO PIR formation might be an ADH isoform.

5-CHO PIR formation from 5-OH PIR by recombinant ADH isoforms

Among 7 human ADH isoforms, ADH1A, ADH1B, ADH1C, ADH4, and ADH5 are expressed in the liver (Di et al., 2021). The amino acid sequence identities between the ADH1 isoforms are greater than 90%, and those between the ADH1s, ADH4, and ADH5 isoforms are approximately 60% (Lee et al., 2006). To investigate the ADH isoforms that catalyze 5-CHO PIR formation from 5-OH PIR, recombinant ADH1A, ADH1B, ADH1C, ADH4, and ADH5 expressed in HEK293T cells were constructed, although ADH5 was not detected by proteomics (Fig. 4C). Western blotting with an anti-ADH antibody confirmed the expression of all ADH isoforms. In addition, a clear band was observed for both pHLM and pHLC, even though ADHs were known to be localized in the cytosol (Duester et al., 1999) (Fig. 5A). Using an anti-ADH4 antibody, a band was observed in recombinant ADH4, as well as in ADH1s, pHLM, and pHLC (Fig. 5A). Using an anti-ADH5 antibody, a band was observed only for the recombinant ADH5, indicating the specificity of this antibody for ADH5 (Fig. 5A). Among the two bands observed in pHLC (Fig. 5A), the band with fast mobility was ADH5, and that with low mobility may be a non-specific protein or post-translationally modified ADH5. ADH5 was not detected in microsomal fractions.

Using recombinant ADH isoforms, 5-OH PIR oxidase activity was evaluated (Fig. 5B). The SEM conjugate and 5-COOH PIR were mostly formed by rADH4, followed by rADH1C

DMD Fast Forward. Published on October 29, 2024 as DOI: 10.1124/dmd.124.001917
This article has not been copyedited and formatted. The final version may differ from this version.

and rADH5 but not by rADH1A or rADH1B. Their formation was also observed in pHLM, although SEM conjugate formation was not detected in pHLC (Fig. 5B). SEM conjugate formation by rADH4 and pHLM fitted to the Michaelis-Menten equation, whereas that by pHLC increased linearly up to 600 μM substrate concentration (Fig. 5C, Table 2). Eadie-Hofstee plots of the activities by rADH4 and pHLM were monophasic with the K_m values, 29.0 ± 4.9 and 59.1 ± 4.6 μM, respectively, whereas that by pHLC was biphasic with K_m values, 94.4 ± 15.3 μM and 2410.1 ± 157.4 μM (Fig. 5C, Table 2). The K_m values of pHLM and the high component of pHLC were relatively close to those of rADH4 (Fig. 5C, Table 2), suggesting that ADH4 in the endoplasmic reticulum and cytosol may contribute to the oxidation of 5-OH PIR. However, the formation of the SEM conjugate and 5-COOH PIR by pHLM was higher than that by pHLC (Fig. 5B) because ADH protein levels were higher in pHLC than in pHLM, as shown using Western blotting (Fig. 5A). The ADH4 activity in pHLC may be underestimated by some HLC components.

5-CHO PIR and 5-COOH PIR formation by HLM or HLC from individual human livers

To investigate whether the lower ADH4 activity in HLC than expected, based on the expressed ADH4 protein level (Figs. 5A and B), was common in all liver fractions, the oxidation of 5-OH PIR was evaluated using microsomes or cytosols prepared in-house from ten individual human livers (Figs. 6A and B). Interestingly, in contrast to the results from the commercially available pHLC and pHLM, the SEM conjugate formations of individual HLC samples were comparable to those of individual HLM samples (Fig. 6A), and the 5-COOH PIR formations of individual HLC samples were significantly higher than those of individual HLM samples (Fig. 6B). These results implied that ADH4 activity in pHLC may be inhibited by certain components. To investigate whether the formation of the SEM conjugate and 5-COOH PIR by HLM was due to enzymes in the contaminated HLC, the activity of cytosolic aldehyde oxidase 1 (AOX1), a typical cytosolic protein, was measured using phthalazine as a substrate. As shown in Fig. 6C, phthalazine oxidase activity was barely detected by HLM but

DMD Fast Forward. Published on October 29, 2024 as DOI: 10.1124/dmd.124.001917
This article has not been copyedited and formatted. The final version may differ from this version.

was clearly detected by HLC. Thus, the formation of the SEM conjugate by HLM was not due to contamination with cytosolic proteins, suggesting that ADH4 in HLM could catalyze the formation of 5-CHO PIR.

Identification of proteins correlated with 5-CHO PIR formation in a panel of 25 individual HLC samples

To further examine the role of ADH in 5-CHO PIR formation, proteins with expressions that correlated with SEM conjugate formation were investigated by untargeted proteomics using a panel of 25 individual HLC samples. Of the 4,552 proteins quantified in our previous study (Kudo et al., 2023), the top ten proteins categorized as oxidoreductases by the EC classification and showing significant correlation coefficients (*rs*) are listed in Table 3. ADH4, ADH6, and malate dehydrogenase 1 are NAD^+-dependent enzymes that catalyze alcohol oxidation. ADH4 showed the second-highest correlation with SEM conjugate formation (rs = 0.772, $P < 0.0001$). ADH6 could not be involved in 5-CHO PIR formation because computational modeling suggests that ADH6 might be highly unstable and behaved like a dead enzyme because of its inability to form a dimer (Östberg et al., 2016). Because malate dehydrogenase 1 was not detected in the purified fraction (Fig. 4C), it was unlikely to be involved in the oxidation of 5-OH PIR in the human liver. The other hepatic ADH isoforms not listed in Table 3, ADH1A (rs = 0.359, P = 0.08), ADH1B (rs = 0.513, $P < 0.01$), ADH1C (rs = 0.114, P = 0.59), and ADH5 (rs = 0.309, P = 0.13) (Fig. 7), did not strongly correlate with SEM conjugate formation. These results suggested that ADH4 largely contributes to 5-CHO PIR formation from 5-OH PIR in the human liver.

Involvement of ALDH1A1 and ALDH2 in the formation of 5-COOH PIR

As shown in Fig. 2B, the formation of 5-COOH PIR by pHLM was completely inhibited by 20 μM disulfiram, suggesting that disulfiram-sensitive ALDH isoforms would be involved in the formation of 5-COOH PIR from 5-CHO PIR. As potential ALDH isoforms, this study focused on ALDH1A1 and ALDH2, which are known to be localized in the cytoplasm and

mitochondria, respectively, as they are the major hepatic ALDH isoforms (Klyosov et al., 1996; Sládek et al., 2003). To investigate whether ALDH1A1 and ALDH2 are involved in the formation of the 5-COOH PIR, siRNAs were transfected into HepG2 cells expressing ADH4 (Pochareddy and Edenberg, 2010). ALDH1A1 and ALDH2 protein levels were significantly decreased by siALDH1A1 and siALDH2 to 9 and 10% of those in the control, respectively (Figs. 8A and B). 5-COOH PIR formation was significantly but moderately decreased by siALDH2 treatment to 61% of the control, but was not altered by siALDH1A1 treatment (Fig. 8C). These results suggest that ALDH2 partially catalyzes the oxidation of 5-CHO PIR, and the other disulfiram-sensitive enzyme(s) are involved in the formation of 5-COOH-PIR.

DMD Fast Forward. Published on October 29, 2024 as DOI: 10.1124/dmd.124.001917
This article has not been copyedited and formatted. The final version may differ from this version.

Discussion

The PIR used for the treatment of IPF is metabolized to 5-OH PIR and subsequently to 5-COOH PIR, which is excreted in the urine at approximately 90% of the dose (Huang et al., 2013). Our previous study showed that the formation of 5-OH PIR from PIR is primarily catalyzed by CYP1A2 and partly by CYP2C19 and CYP2D6 (Zhang et al., 2021). The enzymes that catalyze the oxidation of 5-OH PIR to 5-COOH PIR have not yet been elucidated. Generally, alcohols are oxidized to their corresponding carboxylic acids via aldehyde formation (Di et al., 2021). In this study, we aimed to characterize the reactions and enzymes involved in the formation of 5-COOH PIR from 5-OH PIR in the human liver.

First, 5-COOH PIR was efficiently formed from 5-OH PIR in pHLM in the presence of NAD^+ and was also slightly formed even in the absence of NAD^+ (Fig. 2B). As the 5-COOH PIR was not formed in the absence of enzyme sources (data not shown), NAD^+ included in the liver preparations may proceed the reaction or enzymes not requiring NAD^+ may be involved in the formation of 5-COOH PIR. 5-CHO PIR was detected as an intermediate in the oxidation of 5-OH PIR to 5-COOH PIR by HPLC and LC-MS/MS analyses (Fig. 2). In addition, 5-CHO PIR was detected as a stable conjugate in the presence of SEM (Fig. 3). These results are consistent with those of previous studies reported that losartan and dolutegravir were oxidized to aldehyde metabolites that were trapped by SEM (Iwamura et al., 2011; Zhu et al., 2018).

Possible enzymes that catalyze the formation of aldehydes in an NAD^+-dependent manner are members of the ADH and hydroxysteroid dehydrogenase, as well as retinol dehydrogenases (Di et al., 2021; Bray et al., 2009). Protein purification from HLM identified ADHs with molecular weights of approximately 40 kDa as candidate enzymes that catalyze 5-CHO PIR formation from 5-OH PIR. Proteins with a molecular weight of approximately 25 kDa were also considered candidate enzymes catalyzing the oxidation of 5-OH PIR because the band intensity of approximately 25 kDa in silver staining also increased as the purification steps proceeded (Fig. 4A). However, the band intensity did not correlate with SEM conjugate

formation (Fig. 4B), and proteins of approximately 25 kDa were not observed in the proteomic data of protein purification (Fig. 4C). Therefore, proteins of approximately 25 kDa were excluded from the candidate enzymes in this study. Among the recombinant ADH isoforms, only ADH4 catalyzed 5-CHO PIR formation (Fig 5B). In addition, correlation analysis using 25 individual HLC samples showed a significant positive correlation between the SEM conjugate and relative ADH4 protein expression levels (Fig. 7D). ADH4 is specifically expressed in the liver (Di et al., 2021). The SEM conjugate was not formed in intestinal and renal microsomes (data not shown). These results supported the role of ADH4 in 5-CHO PIR formation in the human liver. Despite the high scores of ADH1 isoforms in the proteomic analysis of the final fraction during protein purification (Fig. 4C), the recombinant ADH1s did not catalyze 5-CHO PIR formation. This result is consistent with the fact that 4-methylpyrazole, a potent inhibitor of ADH1s (Pietruszko, 1975), hardly inhibited SEM conjugate formation by pHLM or pHLC (data not shown). One of the possible reasons why ADH1s were identified as candidate enzymes in the proteomic analysis of purified proteins was their high amino acid identities and similar isoelectric points (ADH1A: 8.26, ADH1B: 8.63, ADH1C: 8.63, and ADH4:8.25, based on the ExPASy database, https://www.expasy.org) with those of ADH4.

The ADH4 protein was detected in both pHLM and pHLC using Western blotting. Nishiya et al. (2016) reported that oxidation of the alcohol metabolite of tivantinib, which is specifically catalyzed by ADH4, was observed in both HLM and HLC. It has been reported that the human *ADH4* gene produces two transcripts via alternative splicing, which are translated to two isoforms with different N-terminus (isoform 1:40.2 kDa, NP_001293100.1, isoform 2:42.6 kDa, NP_000661.2) (Chen et al., 2018). ADH4 isoform 2 has a mitochondrial signal peptide at its N-terminus, suggesting mitochondrial localization (Chen et al., 2018). Western blotting revealed a substantial expression of ATP synthase α-subunit, a mitochondrial marker protein, in pHLM but not in pHLC (Supplemental Fig. 1). This result aligns with a previous report that approximately 14% of microsomal fractions prepared using conventional methods consist of mitochondrial proteins (Wegler et al., 2021). Therefore, the

DMD Fast Forward. Published on October 29, 2024 as DOI: 10.1124/dmd.124.001917
This article has not been copyedited and formatted. The final version may differ from this version.

oxidation of 5-OH PIR and the alcohol metabolite of tivantinib to aldehydes observed in HLM could be due to the contamination of mitochondrial ADH4 isoform 2 in HLM.

Although the purchased pHLC did not show SEM conjugate formation, the HLC prepared in-house showed conjugate formation comparable to that of HLM (Fig. 6A). By kinetic analysis of SEM conjugate formation, individual HLC (No. 6), which showed an average activity among all samples, showed a *K*m value of 67.5 ± 2.8 μM in a monophasic manner in an Eadie-Hofstee plot (Supplemental Fig. 2). This value was close to those of pHLM and rADH4 (Table 2 and Fig. 5D). Furthermore, 5-CHO PIR formation by recombinant ADH4 was substantially decreased by the addition of the purchased pHLC, whereas it was increased by the addition of individual HLC (No. 6) (Supplemental Fig. 3), suggesting that some components in the purchased pHLC inhibit ADH4. Barr et al. (2014) reported that xanthine oxidase activity is substantially low in HLC samples fractionated from livers perfused with a solution containing allopurinol, a potent xanthine oxidase inhibitor, which is used to protect against reperfusion injury. We confirmed through personal communication with the supplier that the livers used to prepare in-house individual HLCs were perfused with University of Wisconsin solution, which contains allopurinol (Janssen et al., 2004). Notably, the xanthine oxidase activity using xanthine as a substrate at a concentration of 10 μM in the individual HLCs was quite low (No. 1 and 6: 28.1 ± 2.5 and 29.1 ± 0.3 pmol/min/mg protein, respectively). In contrast, the activity in pHLC was relatively high (144.5 ± 1.0 pmol/min/mg protein), suggesting that the livers used for pHLC were likely perfused with a different type of perfusate, possibly lacking allopurinol, although the components of the perfusate for pHLC are undisclosed. These differences in perfusate composition may explain the difference in ADH4 activity between the individual HLCs and pHLC (Supplemental Fig. 2). The elucidation of the possible mechanism of low ADH4 activity in pHLC will be the subject of future studies.

In general, ADH-catalyzed oxidation of alcohols to aldehydes is the rate-limiting step in the formation of carboxylic acids (Bosron et al., 1986). In ten individual HLC and HLM, approximately 6-fold inter-individual variability was observed in the formation of the 5-

DMD Fast Forward. Published on October 29, 2024 as DOI: 10.1124/dmd.124.001917
This article has not been copyedited and formatted. The final version may differ from this version.

COOH PIR from the 5-OH PIR (Fig. 6B). Wei et al. (2012) reported an approximately 7-fold variation in ADH4 mRNA expression in human hepatocytes from 15 donors, which was close to the ADH4 protein levels observed in our study (Fig. 7D). Thus, inter-individual variability in 5-COOH PIR formation by ten individual HLC and HLM could be explained by inter-individual variation in ADH4 expression levels or activity. Edenberg et al. (1999) identified three single nucleotide polymorphisms (SNPs) in the promoter of *ADH4* gene and showed, using a luciferase assay, that the SNP (-75A>C, rs1800759), whose allele frequencies were 0.58 (Caucasian), 0.79 (Asian), 0.24 (African), and 0.40 (Hispanic) according to the dbSNP database, decreased promoter activity by half (Edenberg et al., 1999). Another study reported that miR-148a positively regulates ADH4 mRNA and protein levels by increasing ADH4 mRNA stability in an ARGONAUTE1-dependent manner (Luo et al., 2021). Such genetic and epigenetic factors affecting ADH4 expression may cause inter-individual variations in the formation of 5-COOH PIR from 5-OH PIR.

5-COOH PIR formation by recombinant ADH4 (Fig. 5B) was significantly inhibited by disulfiram, which did not inhibit ADH4 activity (data not shown), suggesting that enzyme(s) endogenously expressed in HEK293T cells could catalyze 5-COOH PIR formation from 5-CHO PIR. Disulfiram significantly decreased 5-COOH PIR formation but increased 5-CHO PIR formation by pHLM (Fig. 2B), suggesting that disulfiram-sensitive enzymes were involved in the formation of 5-COOH PIR. Among ALDH isoforms, only ALDH1A1 and ALDH2 have been reported to be inhibited by disulfiram and are highly expressed in the liver (Klyosov et al., 1996; Ma et al., 2011). Transfection with siALDH2 significantly but moderately decreased 5-COOH PIR formation from 5-OH PIR in HepG2 cells (Fig. 8). Thus, 5-COOH PIR formation by HLM (Fig. 5B) can be partially attributed to mitochondrial ALDH2 (Ma et al., 2011). Another possibility is that other disulfiram-sensitive enzymes in HLM may be involved in the formation of 5-COOH PIR. Since information on enzymes catalyzing the oxidation of aldehyde-containing drugs, including ALDH isoforms, is limited, the identification of enzymes catalyzing 5-COOH PIR formation from 5-CHO PIR can provide new insights into drug metabolism.

DMD Fast Forward. Published on October 29, 2024 as DOI: 10.1124/dmd.124.001917
This article has not been copyedited and formatted. The final version may differ from this version.

In conclusion, we found that the oxidation of 5-OH PIR proceeds in two steps: conversion to 5-CHO PIR by ADH4 in the microsomal and cytosolic fractions, and subsequent oxidation to 5-COOH PIR by disulfiram-sensitive enzymes, including ALDH2. This study contributes to an improved understanding of PIR metabolism.

Footnotes

This work was supported by Mochida Memorial Foundation for Medical and Pharmaceutical Research, World Premier International Research Center Initiative (WPI) and WISE Program for Nano-Precision Medicine, Science, and Technology of Kanazawa University by MEXT.
No author has an actual or perceived conflict of interest with the contents of this article.

Acknowledgments

The authors would like to thank Dr. Takashi Kudo, Mr. Gaku Morinaga, Dr. Akiko Matsui, and Dr. Naoki Ishiguro of Nippon Boehringer Ingelheim Co. for their collaboration and valuable contributions to LC-tandem mass spectrometry–based untargeted proteomics.

DMD Fast Forward. Published on October 29, 2024 as DOI: 10.1124/dmd.124.001917
This article has not been copyedited and formatted. The final version may differ from this version.

Data Availability Statement

The authors declare that all the data supporting the findings of this study are available within the paper.

DMD Fast Forward. Published on October 29, 2024 as DOI: 10.1124/dmd.124.001917
This article has not been copyedited and formatted. The final version may differ from this version.

Authorship Contributions

Participated in research design: Fukami, Nakano, and Nakajima

Conducted experiments: Sato and Shimomura

Performed data analysis: Sato, Shimomura, and Zhang

Wrote or contributed to the writing of the manuscript: Sato, Fukami, and Nakajima

References

Amano T, Fukami T, Ogiso T, Hirose D, Jones JP, Taniguchi T, and Nakajima M (2018) Identification of enzymes responsible for dantrolene metabolism in the human liver: A clue to uncover the cause of liver injury. *Biochem Pharmacol* **151**: 69–78.

Barr JT, Choughule KV, Nepal S, Wong T, Chaudhry AS, Joswig-Jones CA, Zientek M, Strom SC, Schuetz EG, Thummel KE, and Jones JP (2014) Why do most human liver cytosol preparations lack xanthine oxidase activity? *Drug Metab Dispos* **42**: 695–9.

Bosron WF and Li TK (1986) Genetic polymorphism of human liver alcohol and aldehyde dehydrogenases, and their relationship to alcohol metabolism and alcoholism. *Hepatology* **6**: 502–510.

Bradford MM (1976) A rapid and sensitive method for the quantitation of microgram quantities of protein utilizing the principle of protein-dye binding. *Anal Biochem* **72**: 248–254.

Bray JE, Marsden BD, and Oppermann U (2009) The human short-chain dehydrogenase/reductase (SDR) superfamily: a bioinformatics summary. *Chem Biol Interact* **178**: 99–109.

Chen W, Moore J, Ozadam H, Shulha HP, Rhind N, Weng Z, and Moore MJ (2018) Transcriptome-wide Interrogation of the functional intronome by spliceosome profiling. *Cell* **173**: 1031–1044.

Di L, Balesano A, Jordan S, and Shi SM (2021) The role of alcohol dehydrogenase in drug metabolism: beyond ethanol oxidation. *AAPS J* **23**: 20.

Duester G, Farrés J, Felder MR, Holmes RS, Höög JO, Parés X, Plapp BV, and Yin SJ, Jörnvall H (1999) Recommended nomenclature for the vertebrate alcohol dehydrogenase gene family. *Biochem Pharmacol* **58**: 389–395.

Edenberg HJ, Jerome RE, and Li M (1999) Polymorphism of the human alcohol

dehydrogenase 4 *(ADH4)* promoter affects gene expression. *Pharmacogenetics* **9**: 25–30.

Fukami T, Yokoi T, and Nakajima M (2022) Non-P450 drug-metabolizing enzymes: contribution to drug disposition, toxicity, and development. *Annu Rev Pharmacol Toxicol* **62**: 405–425.

Harrison R (2002) Structure and function of xanthine oxidoreductase: where are we now? *Free Radic Biol Med* **33**: 774–797.

Hirano A, Kanehiro A, Ono K, Ito W, Yoshida A, Okada C, Nakashima H, Tanimoto Y, Kataoka M, Gelfand EW, and Tanimoto M (2006) Pirfenidone modulates airway responsiveness, inflammation, and remodeling after repeated challenge. *Am J Respir Cell Mol Biol* **35**: 366–377.

Huang NY, Ding L, Wang J, Zhang QY, Liu X, Lin HD, and Hua WY. (2013) Pharmacokinetics, safety and tolerability of pirfenidone and its major metabolite after single and multiple oral doses in healthy Chinese subjects under fed conditions. *Drug Res (Stuttg)* **63**: 388–395.

Inoue K, Fukuda K, Yoshimura T, and Kusano K (2015) Comparison of the reactivity of trapping reagents toward electrophiles: cysteine derivatives can be bifunctional trapping reagents. *Chem Res Toxicol* **28**:1546–1555.

Iwamura A, Fukami T, Hosomi H, Nakajima M, and Yokoi T (2011) CYP2C9-mediated metabolic activation of losartan detected by a highly sensitive cell-based screening assay. *Drug Metab Dispos* **39**: 838–846.

Janssen H, Janssen PH, Broelsch CE (2004) UW is superior to Celsior and HTK in the protection of human liver endothelial cells against preservation injury. *Liver Transpl* 10: 1514–1523.

Klyosov AA, Rashkovetsky LG, Tahir MK, and Keung WM (1996) Possible role of liver cytosolic and mitochondrial aldehyde dehydrogenases in acetaldehyde metabolism.

Biochemistry **35**: 4445–4456.

Kobayashi Y, Fukami T, Nakajima A, Watanabe A, Nakajima M, and Yokoi T (2012) Species differences in tissue distribution and enzyme activities of arylacetamide deacetylase in human, rat, and mouse. *Drug Metab Dispos* **40**: 671–679.

Kudo T, Hashiba S, Fukami T, Morinaga G, Nishiyama K, Ichida H, Hirosawa K, Matsui A, Ishiguro N, and Nakajima M (2023) Development and validation of a proteomic correlation profiling technique to detect and identify enzymes involved in metabolism of drugs of concern. *Drug Metab Dispos* **51**: 824–832.

Lee SP, Chiang CP, Lee SL, Hsia YJ, Chuang TL, Lin JC, Liang SC, Nieh S, and Yin SJ (2006) Immunochemical features in the classification of human alcohol dehydrogenase family. *Alcohol* **39**:13–20.

Luo J, Hou Y, Ma W, Xie M, Jin Y, Xu L, Li C, Wang Y, Chen J, Chen W, Zheng Y, Yu D (2021) A novel mechanism underlying alcohol dehydrogenase expression: hsa-miR-148a-3p promotes *ADH4* expression via an AGO1-dependent manner in control and ethanol-exposed hepatic cells. *Biochem Pharmacol* **189**: 114458.

Ma I and Allan AL (2011) The role of human aldehyde dehydrogenase in normal and cancer stem cells. *Stem Cell Rev* **7**: 292–306.

Nishiya Y, Nakai D, Urasaki Y, Takakusa H, Ohsuki S, Iwano Y, Yasukochi T, Takayama T, Bazyo S, Oza C, Kurihara A, Savage RE, and Izumi T (2016) Stereoselective hydroxylation by CYP2C19 and oxidation by ADH4 in the in vitro metabolism of tivantinib. *Xenobiotica* **46**: 967–976.

O'Brien PJ, Siraki AG, and Shangari N (2005) Aldehyde sources, metabolism, molecular toxicity mechanisms, and possible effects on human health. *Crit Rev Toxicol* **35**: 609–662.

Ogiso T, Fukami T, Zhongzhe C, Konishi K, Nakano M, and Nakajima M (2021) Human superoxide dismutase 1 attenuates quinoneimine metabolite formation from

mefenamic acid. *Toxicology* **448**: 152648.

Östberg LJ, Persson B, and Höög JO (2016) Computational studies of human class V alcohol dehydrogenase - the odd sibling. *BMC Biochem* **17**: 16.

Pietruszko R (1975) Human liver alcohol dehydrogenase--inhibition of methanol activity by pyrazole, 4-methylpyrazole, 4-hydroxymethylpyrazole and 4-carboxypyrazole. *Biochem Pharmacol* **24**: 1603–1607.

Pochareddy S and Edenberg HJ (2010) Identification of a FOXA-dependent enhancer of human alcohol dehydrogenase 4 (*ADH4*). *Gene* **460**:1–7.

Richeldi L, Collard HR, and Jones MG (2017) Idiopathic pulmonary fibrosis. *Lancet* **389**: 1941–1952.

Sládek NE (2003) Human aldehyde dehydrogenases: potential pathological, pharmacological, and toxicological impact. *J Biochem Mol Toxicol* **17**: 7–23.

Terao M, Romão MJ, Leimkühler S, Bolis M, Fratelli M, Coelho C, Santos-Silva T, and Garattini E (2016) Structure and function of mammalian aldehyde oxidases. *Arch Toxicol* **90**: 753–780.

Tomlinson AJ, Johnson KL, Lam-Holt J, Mays DC, Lipsky JJ, and Naylor S (1997) Inhibition of human mitochondrial aldehyde dehydrogenase by the disulfiram metabolite *S*-methyl-*N*,*N*-diethylthiocarbamoyl sulfoxide: structural characterization of the enzyme adduct by HPLC-tandem mass spectrometry. *Biochem Pharmacol* **54**: 1253–1260.

Wegler C, Matsson P, Krogstad V, Urdzik J, Christensen H, Andersson TB, and Artursson P (2021) Influence of proteome profiles and intracellular drug exposure on differences in CYP activity in donor-matched human liver microsomes and hepatocytes. *Mol Pharm* **18**: 1792–1805.

Wei RR, Zhang MY, Rao HL, Pu HY, Zhang HZ, and Wang HY (2012) Identification of ADH4 as a novel and potential prognostic marker in hepatocellular carcinoma. *Med*

Oncol **29**: 2737–2743.

Zhang Y, Sato R, Fukami T, Nakano M, and Nakajima M (2021) Pirfenidone 5-hydroxylation is mainly catalysed by CYP1A2 and partly catalysed by CYP2C19 and CYP2D6 in the human liver. *Xenobiotica* **51**: 1–8.

Zanger UM and Schwab M (2013) Cytochrome P450 enzymes in drug metabolism: regulation of gene expression, enzyme activities, and impact of genetic variation. *Pharmacol Ther* **138**: 103–141.

Zhu J, Wang P, Li F, Lu J, Shehu AI, Xie W, McMahon D, and Ma X (2018) CYP1A1 and 1B1-mediated metabolic pathways of dolutegravir, an HIV integrase inhibitor. *Biochem Pharmacol* **158**: 174–184.

DMD Fast Forward. Published on October 29, 2024 as DOI: 10.1124/dmd.124.001917
This article has not been copyedited and formatted. The final version may differ from this version.

Table 1. Primer sequences used for reverse transcription (RT)-PCR

Enzyme	Primer	Sequence (5' → 3')
ADH1A	S	CTCACCAGTCTCCTGGTCT
	AS	AGACTGCCACAAGGGAAAA
ADH1B	S	GGGCAGAGAAGACAGAAACG
	AS	GGGGAAGGCATCTCTATTGC
ADH1C	S	TCCACAAGTACTCACCAGC
	AS	GAAAACTGCTACAAGGGAAGG
ADH4	S	GCAATTATCTGACTCAGGTTAT
	AS	TCAAAAGATGAGGATTGTTCGGAC
ADH5	S	GAATCCGTGAACATGGCGA
	AS	TATCACATCACGACAGGATGGA

S, sense primer; AS, antisense primer

DMD Fast Forward. Published on October 29, 2024 as DOI: 10.1124/dmd.124.001917
This article has not been copyedited and formatted. The final version may differ from this version.

Table 2. Kinetic parameters for 5-OH PIR oxidase activities by pHLM, pHLC, and recombinant ADH4

	K_m	V_{max}	CL_{int}
	μM	Area/min/mg protein	Area/min/mg/μM
pHLM	59.1 ± 4.6	11394.0 ± 251.4	192.8 ± 20.6
pHLC	94.4 ± 15.3[a]	477.7 ± 200.2[a]	5.0 ± 1.7[a]
	2410.1 ± 157.4[b]	20230.3 ± 1676.5[b]	8.4 ± 0.52[b]
rADH4	29.0 ± 4.9	17094.7 ± 317.0	599.3 ± 85.4

[a]High affinity component, [b]low affinity component

Date represents the mean ± SD of triplicate determinations.

DMD Fast Forward. Published on October 29, 2024 as DOI: 10.1124/dmd.124.001917
This article has not been copyedited and formatted. The final version may differ from this version.

Table 3. Proteins with high correlation coefficients in SEM conjugate formation

Rank	Protein	*rs* value
1	Ketimine reductase mu-crystallin (CRYM)	0.781
2	Alcohol dehydrogenase 4 (ADH4)	0.772
3	Phospholipid hydroperoxide glutathione peroxidase (GPX 4)	0.736
4	C-terminal-binding protein 1 (CTBP1)	0.721
5	C-1-tetrahydrofolate synthase, cytoplasmic (MTHFD1)	0.645
6	Short-chain dehydrogenase/reductase 3 (DHRS3)	0.618
7	Alcohol dehydrogenase 6 (ADH6)	0.608
8	2-aminomuconic semialdehyde dehydrogenase (ALDH8A1)	0.604
9	Ribosomal oxygenase 2 (RIOX2)	0.594
10	Malate dehydrogenase, cytoplasmic (MDH1)	0.587

DMD Fast Forward. Published on October 29, 2024 as DOI: 10.1124/dmd.124.001917
This article has not been copyedited and formatted. The final version may differ from this version.

Figure Legends

Fig. 1. Proposed metabolic pathways of PIR in the human liver.

Fig. 2. Formation of 5-COOH PIR from 5-OH PIR by pHLM or pHLC in the presence of cofactors, and detection of 5-CHO PIR using HPLC and LC-MS/MS. (A) Effects of NAD^+, NADH, $NADP^+$, or NADPH on the formation of 5-COOH PIR from 5-OH PIR. Each column represents the mean ± SD of triplicate determinations. ND: not detectable. (B) HPLCs of the metabolites formed upon the incubation of 5-OH PIR and pHLM in the presence of NAD^+ or disulfiram. (C) Chromatograms of Q1 scan in the range *m/z* 190–220 and MS spectra of peaks 1 and 2 in the sample in the presence of HLM and NAD^+. (D) Chromatograms of SIM set at *m/z* 216.1 (upper panel) and 200.1 (lower panel). (E) Product ions obtained from the precursor ion at *m/z* 216.1 (upper panel) and 200.1 (lower panel) in the range *m/z* 30–180.

Fig. 3. Detection of 5-CHO PIR as a stable conjugate using SEM and HLM. (A) HPLCs of 5-OH PIR and 5-CHO PIR in the presence or absence of SEM. (B) Chromatograms of the Q1 scan in the range *m/z* 230–280 and MS spectra of peak 3 in the sample in the presence of NAD^+ and SEM. (C) Chromatogram of SIM set at *m/z* 257.2. (D) Product ions obtained from the precursor ion at *m/z* 257.2 in the range *m/z* 100–200.

Fig. 4. Isolation of candidate enzymes catalyzing 5-CHO PIR formation by protein purification from HLM. (A) SDS-PAGE and silver staining of the fractions obtained from a series of the purification steps (each lane, 1.3 μg of protein). (B) SEM conjugation of each fraction and relative intensities of the two protein bands (42 and 25 kDa). Intensities of each protein band are shown relative to the highest intensity value in each protein band. Each column represents the mean ± SD of triplicate determinations. (C) Top ten proteins with high SEQUEST HT scores in the final fraction of protein purification.

Fig. 5. SEM conjugate of 5-CHO PIR and 5-COOH PIR formations by rADH isoforms. (A) Western blot analysis of homogenates from HEK293T cells overexpressing human ADH1A, ADH1B, ADH1C, ADH4, or ADH5, pHLM, and pHLC using anti-human ADH1, ADH4, and ADH5 antibodies (each lane, 3 μg of protein). (B) Formation of SEM conjugate and 5-COOH PIR from 5-OH PIR by rADH isoforms, pHLM, and pHLC. Concentration of 5-OH PIR was 50 μM. Each column represents the mean ± SD of triplicate determinations. ND: not detectable. (C) S-V and Eadie-Hofstee plots of the SEM conjugate formation by pHLM, pHLC, or rADH4 in the presence of 20 μM disulfiram. 5-OH PIR at 5–600 μM was incubated with 0.5 mg/mL pHLM, pHLC, or rADH4. Each point represents the mean ± SD of triplicate determinations.

Fig. 6. SEM conjugate of 5-CHO PIR and 5-COOH PIR formation from 5-OH PIR and phthalazine oxidase activity in a panel of ten individual human livers. (A) SEM conjugate and (B) 5-COOH PIR formation by HLM and HLC were measured using HPLC. The substrate concentration was set to be 50 μM. (C) Phthalazine oxidase activities by HLM and HLC were measured using HPLC as a marker activity for AOX1. Each column represents the average of duplicate determinations.

Fig. 7. Correlation analyses between SEM conjugate of 5-CHO PIR formations and relative protein levels of ADH isoforms determined using proteomics in a panel of 25 individual HLC samples. Protein levels of (A) ADH1A, (B) ADH1B, (C) ADH1C, (D) ADH4, and (E) ADH5 determined using proteomics are represented as relative levels to the sample with the lowest expression levels. SEM conjugate formation from 5-OH PIR was measured at 50 μM in the presence of 20 μM disulfiram.

Fig. 8. Effects of the knockdown of ALDH1A1 or ALDH2 on 5-COOH PIR formation in HepG2 cells. (A) ALDH1A1 and (B) ALDH2 protein levels in HepG2 cells 72 h after transfection with 5 nM siControl, siALDH1A1, or siALDH2 were determined using Western

DMD Fast Forward. Published on October 29, 2024 as DOI: 10.1124/dmd.124.001917
This article has not been copyedited and formatted. The final version may differ from this version.

blotting, and normalized to GAPDH level. Each column represents the mean ± SD of triplicate determinations. $^{***}P < 0.001$, compared to siControl. (C) Formation of 5-COOH PIR in siALDH1A1-, siALDH2-, or siControl-transfected HepG2 cells treated with 5-OH PIR for 12 h. Each column represents the mean ± SD of triplicate determinations. $^{**}P < 0.01$, compared to siControl.

Fig. 1

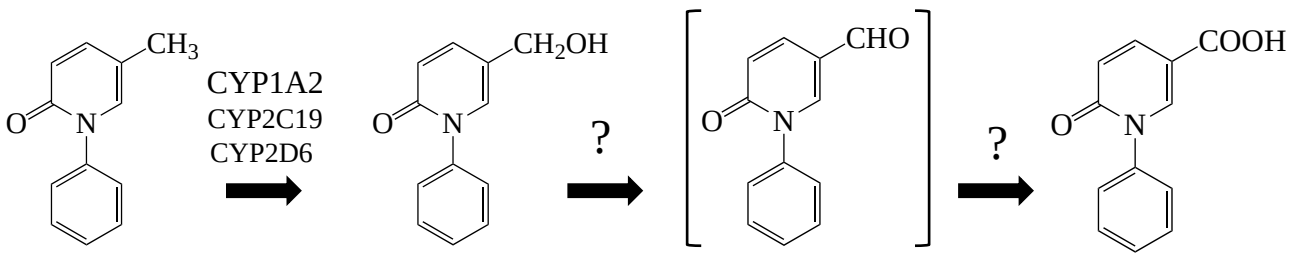

Pirfenidone (PIR)

5-Hydroxylpirfenidone (5-OH PIR)

Pirfenidone aldehyde (5-CHO PIR)

5-Carboxylpirfenidone (5-COOH PIR)

Fig. 2

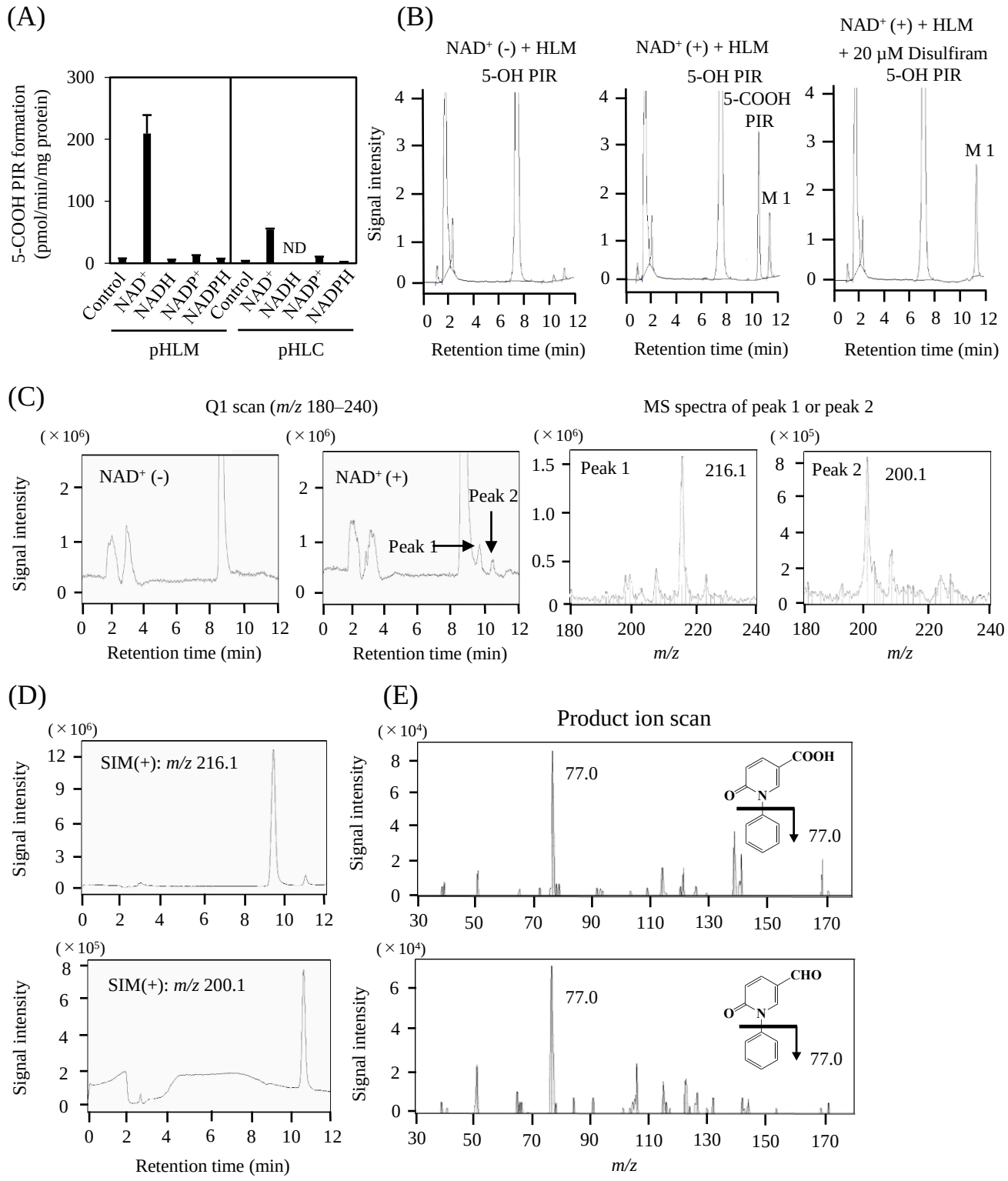
(A)
5-COOH PIR formation (pmol/min/mg protein)
300
200
100
0
ND
Control
NAD+
NADH
NADP+
NADPH
Control
NAD+
NADH
NADP+
NADPH
pHLM
pHLC
(B)
NAD+ (-) + HLM
5-OH PIR
NAD+ (+) + HLM
5-OH PIR
5-COOH PIR
M 1
NAD+ (+) + HLM
+ 20 μM Disulfiram
5-OH PIR
M 1
Signal intensity
Retention time (min)
(C)
Q1 scan (m/z 180–240)
MS spectra of peak 1 or peak 2
(×10^6)
NAD+ (-)
NAD+ (+)
Peak 1
Peak 2
(×10^6)
(×10^6)
Peak 1
216.1
(×10^5)
Peak 2
200.1
Signal intensity
Retention time (min)
m/z
(D)
(×10^6)
SIM(+): m/z 216.1
(×10^5)
SIM(+): m/z 200.1
Signal intensity
Retention time (min)
(E)
Product ion scan
(×10^4)
77.0
COOH
77.0
(×10^4)
77.0
CHO
77.0
Signal intensity
m/z

Fig. 3

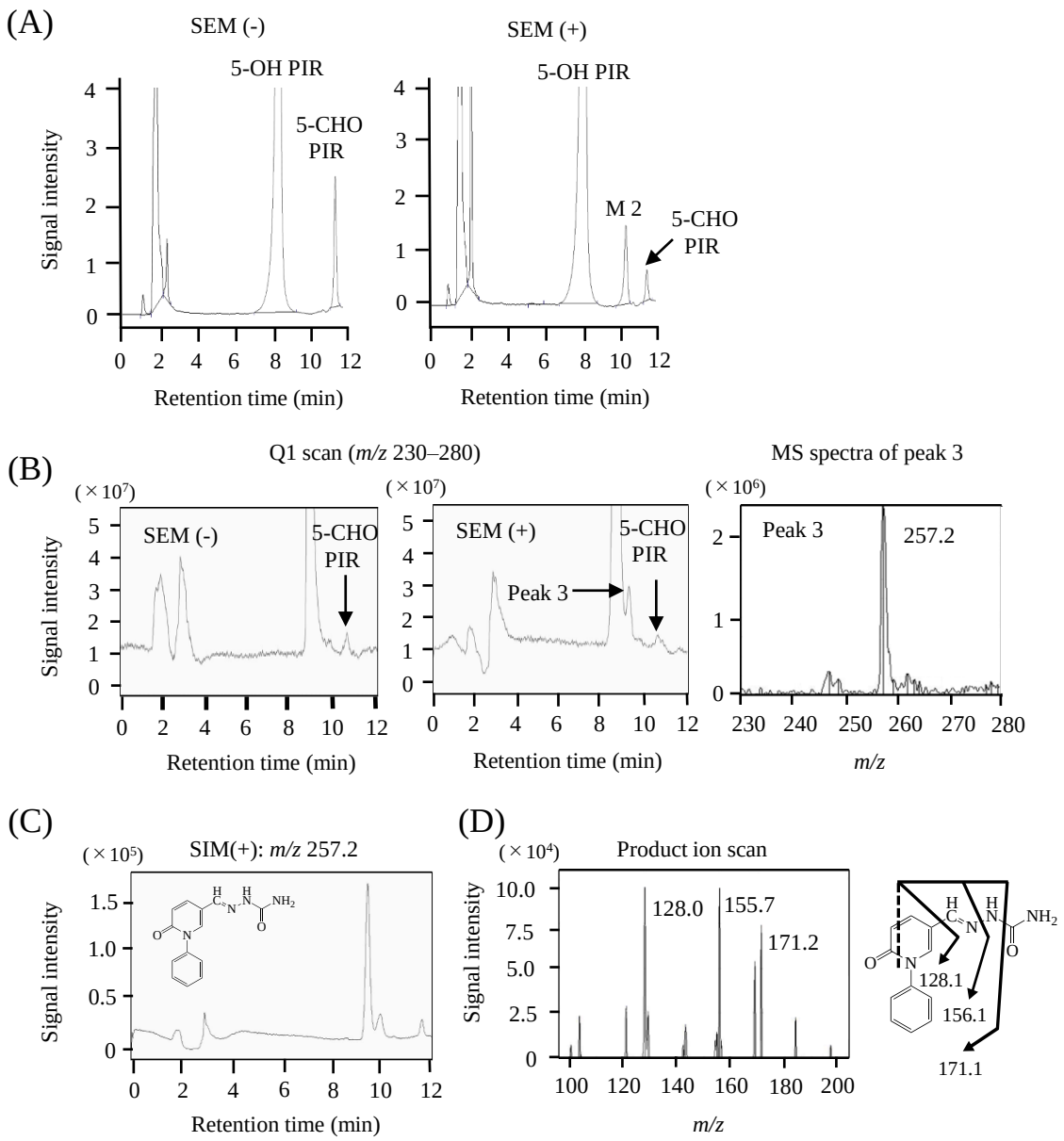
(A)
SEM (-)
5-OH PIR
5-CHO PIR
SEM (+)
5-OH PIR
M 2
5-CHO PIR
Signal intensity
Retention time (min)
(B)
Q1 scan (m/z 230–280)
MS spectra of peak 3
(×10^7)
(×10^6)
SEM (-)
5-CHO PIR
SEM (+)
Peak 3
5-CHO PIR
Peak 3
257.2
Signal intensity
Retention time (min)
m/z
(C)
(D)
(×10^5)
SIM(+): m/z 257.2
(×10^4)
Product ion scan
128.0
155.7
171.2
128.1
156.1
171.1
Signal intensity
Retention time (min)
m/z

Fig. 4

(A)

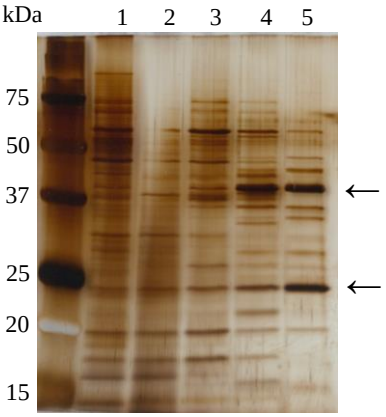

1: Solubilized HLM
2: 50-70% Ammonium sulfate precipitated fraction
3: DEAE Sepharose fraction (pH 8.5)
4: DEAE Sepharose fraction (pH 9.0)
5: Hydroxyapatite fraction

(B)

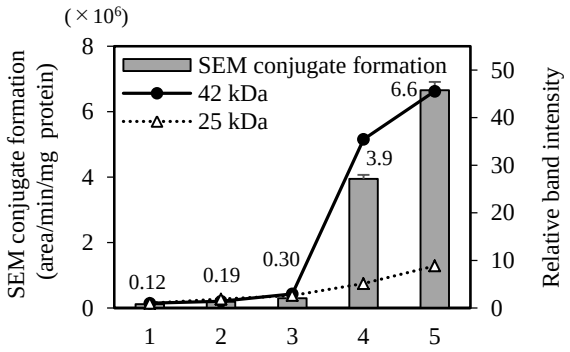

	Relative band intensity				
42kDa	1.0	1.4	3.0	35.5	45.6
25kDa	1.0	1.9	2.6	5.2	8.9

(C)

Protein	MW [kDa]	Score SEQUEST HT
Alcohol dehydrogenase 4	42.6	677.56
Alcohol dehydrogenase 1B	39.8	657.87
Alcohol dehydrogenase 1C	39.8	616.86
Alcohol dehydrogenase 1A	39.8	505.87
Argininosuccinate synthase	46.5	346.75
Carboxylesterase 1	62.6	331.90
Malate dehydrogenase 2	35.5	321.75
Prostaglandin reductase 1	35.8	321.19
Alpha-enolase	47.1	296.96
Glutamate dehydrogenase 1	61.4	176.25

Fig. 5

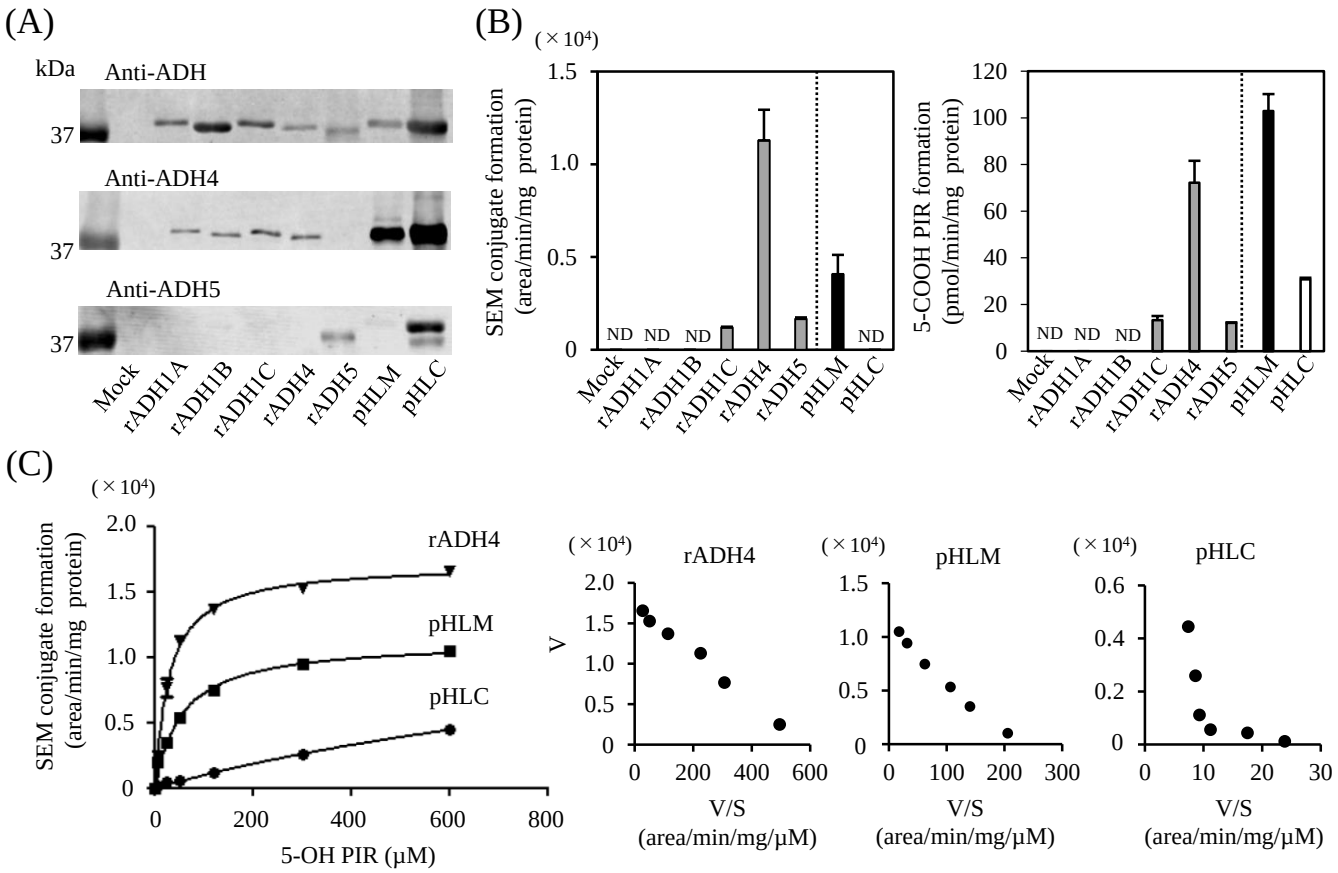
(A)
kDa
Anti-ADH
37
Anti-ADH4
37
Anti-ADH5
37
Mock
rADH1A
rADH1B
rADH1C
rADH4
rADH5
pHLM
pHLC
(B)
(×10⁴)
SEM conjugate formation (area/min/mg protein)
1.5
1.0
0.5
0
ND ND ND ND
5-COOH PIR formation (pmol/min/mg protein)
120
100
80
60
40
20
0
ND ND ND
(C)
(×10⁴)
SEM conjugate formation (area/min/mg protein)
2.0
1.5
1.0
0.5
0
rADH4
pHLM
pHLC
0 200 400 600 800
5-OH PIR (μM)
(×10⁴)
rADH4
V
2.0
1.5
1.0
0.5
0
0 200 400 600
V/S
(area/min/mg/μM)
(×10⁴)
pHLM
1.5
1.0
0.5
0
0 100 200 300
V/S
(area/min/mg/μM)
(×10⁴)
pHLC
0.6
0.4
0.2
0
0 10 20 30
V/S
(area/min/mg/μM)

Fig. 6

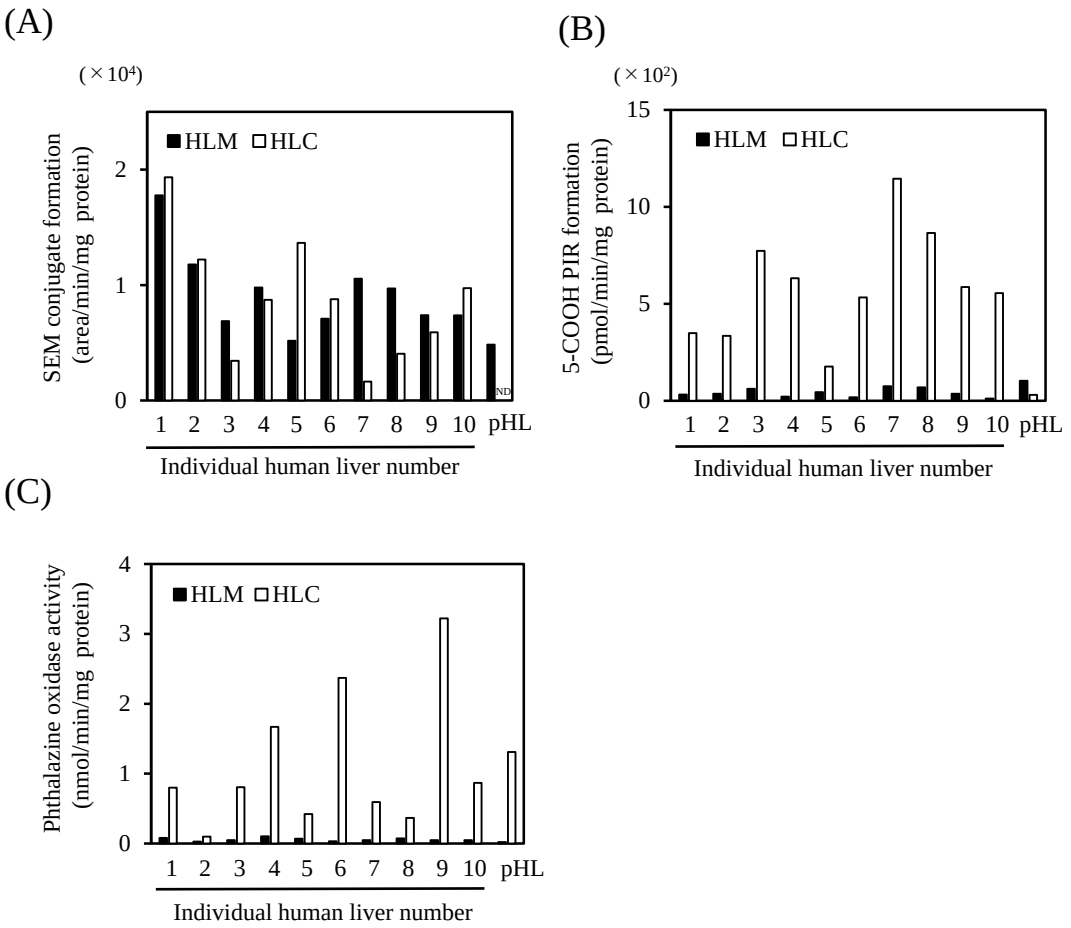
(A)
(×10⁴)
SEM conjugate formation (area/min/mg protein)
HLM HLC
2
1
0
ND
1 2 3 4 5 6 7 8 9 10 pHL
Individual human liver number
(B)
(×10²)
5-COOH PIR formation (pmol/min/mg protein)
HLM HLC
15
10
5
0
1 2 3 4 5 6 7 8 9 10 pHL
Individual human liver number
(C)
Phthalazine oxidase activity (nmol/min/mg protein)
HLM HLC
4
3
2
1
0
1 2 3 4 5 6 7 8 9 10 pHL
Individual human liver number

Fig. 7

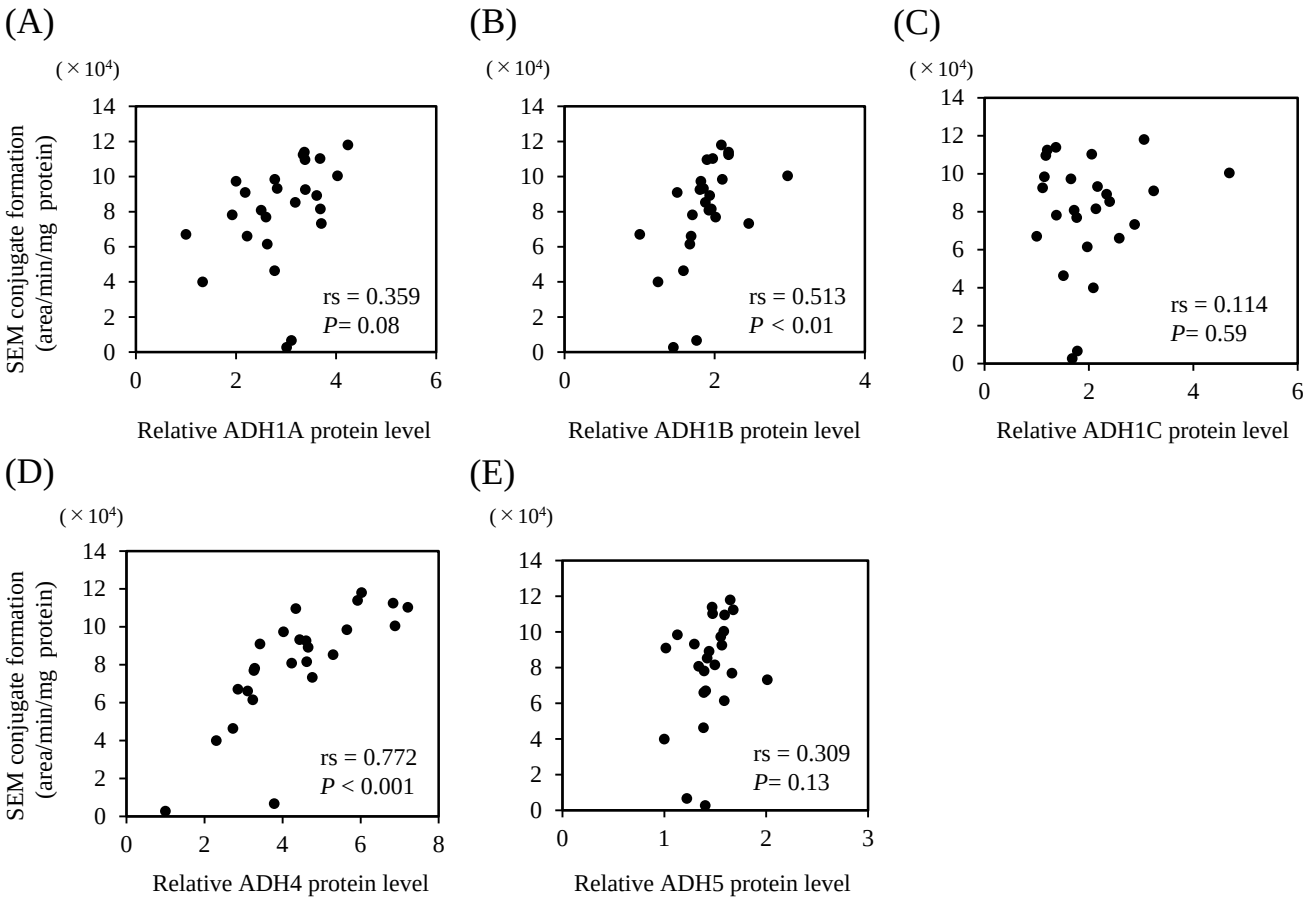
(A)
(×10⁴)
SEM conjugate formation (area/min/mg protein)
rs = 0.359
P= 0.08
Relative ADH1A protein level
(B)
(×10⁴)
rs = 0.513
P < 0.01
Relative ADH1B protein level
(C)
(×10⁴)
rs = 0.114
P= 0.59
Relative ADH1C protein level
(D)
(×10⁴)
SEM conjugate formation (area/min/mg protein)
rs = 0.772
P < 0.001
Relative ADH4 protein level
(E)
(×10⁴)
rs = 0.309
P= 0.13
Relative ADH5 protein level

Fig. 8

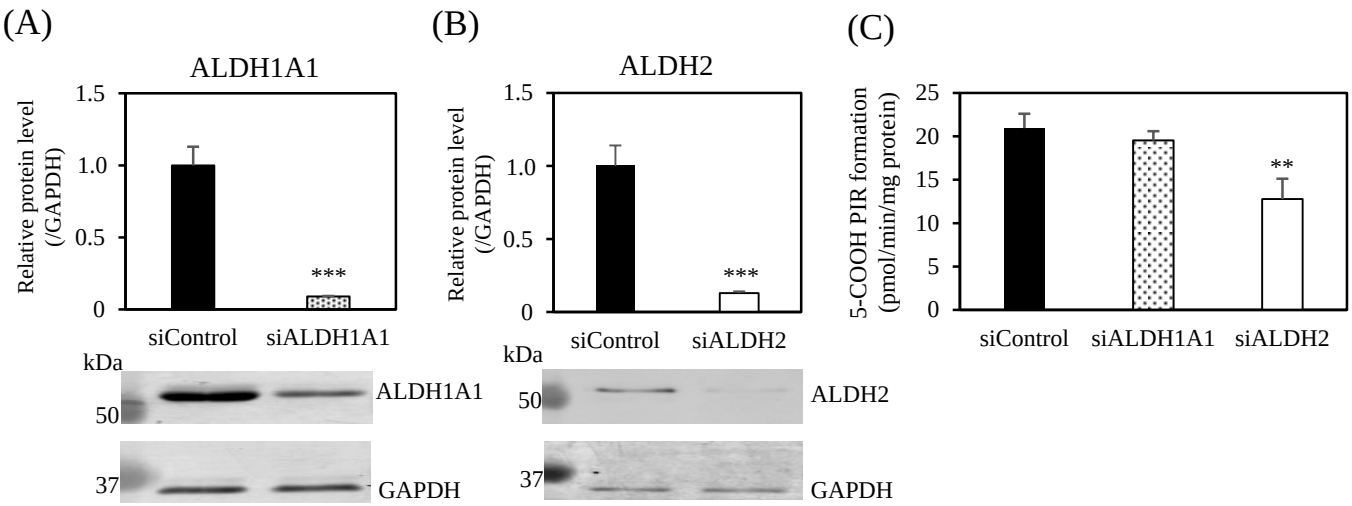
(A)
ALDH1A1
Relative protein level (/GAPDH)
1.5
1.0
0.5
0
***
siControl
siALDH1A1
kDa
50
ALDH1A1
37
GAPDH
(B)
ALDH2
Relative protein level (/GAPDH)
1.5
1.0
0.5
0
***
siControl
siALDH2
kDa
50
ALDH2
37
GAPDH
(C)
5-COOH PIR formation (pmol/min/mg protein)
25
20
15
10
5
0
**
siControl
siALDH1A1
siALDH2

Drug Metab Dispos

Characterization of human alcohol dehydrogenase 4 and aldehyde dehydrogenase 2 as enzymes involved in the formation of 5-carboxylpirfenidone, a major metabolite of pirfenidone

Rei Sato[1], Tatsuki Fukami[1,2], Kazuya Shimomura[1], Yongjie Zhang[3], Masataka Nakano[1,2], and Miki Nakajima[1,2]

[1]Drug Metabolism and Toxicology, Faculty of Pharmaceutical Sciences, and

[2]WPI Nano Life Science Institute (WPI-NanoLSI), Kanazawa University, Kanazawa, Japan

[3]Clinical Pharmacokinetics Laboratory, School of Basic Medicine and Clinical Pharmacy, China Pharmaceutical University, Nanjing, China

Supplemental Table 1. Characteristics of 27 donors of liver used in the present study.

No.	Sex	Age (yr)	Ethnicity	Cause of death	Fig. 6	Fig. 7
1	F	33	H	Intracerebral hematoma	✓	✓
2	M	68	C	Head trauma	✓	✓
3	M	46	C	Oxygen deficiency	✓	✓
4	M	68	C	Cerebrovascular accident	✓	✓
5	F	35	H	Intracerebral hematoma	✓	
6	M	52	C	Cerebrovascular accident	✓	✓
7	M	36	C	Suicide	✓	✓
8	M	54	C	Cerebrovascular accident	✓	
9	M	53	C	Rupture of aneurysm	✓	✓
10	M	60	C	Cerebrovascular accident		✓
11	F	41	C	Intracerebral hematoma		✓
12	F	34	B	Cerebrovascular accident		✓
13	F	59	C	Traffic accident		✓
14	F	52	A	Cerebrovascular accident		✓
15	M	53	C	Rupture of aneurysm		✓
16	M	16	C	Head trauma		✓
17	M	62	A	Rupture of aneurysm		✓
18	F	47	C	Cerebrovascular accident		✓
19	M	46	C	Oxygen deficiency		✓
20	M	52	C	Cerebrovascular accident		✓
21	M	57	A	Cerebrovascular accident		✓
22	F	47	C	S/P code		✓
23	F	51	A	Cerebrovascular accident		✓
24	M	43	C	Cerebrovascular accident		✓
25	M	33	C	Head trauma		✓
26	F	47	C	Cerebrovascular accident		✓
27	F	32	H	Subarachnoid hemorrhage		✓

M, Male; F, Female; A, Asian; B, Black; C, Caucasian; H, Hispanic

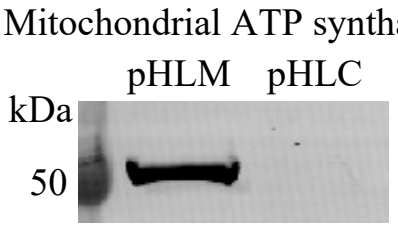

Supplemental Figure 1. Western blotting of mitochondrial ATP synthase α-subunit in pHLM or pHLC. Mitochondrial ATP synthase α-subunit is a mitochondrial marker protein. pHLM or pHLC (each lane, 10 μg of protein) were separated on a 10% polyacrylamide gel and electrotransferred onto a polyvinylidene difluoride (PVDF) membranes. The membrane was probed with a primary antibody against mitochondrial ATP synthase α-subunit, followed by the corresponding fluorescent dye-conjugated secondary antibody.

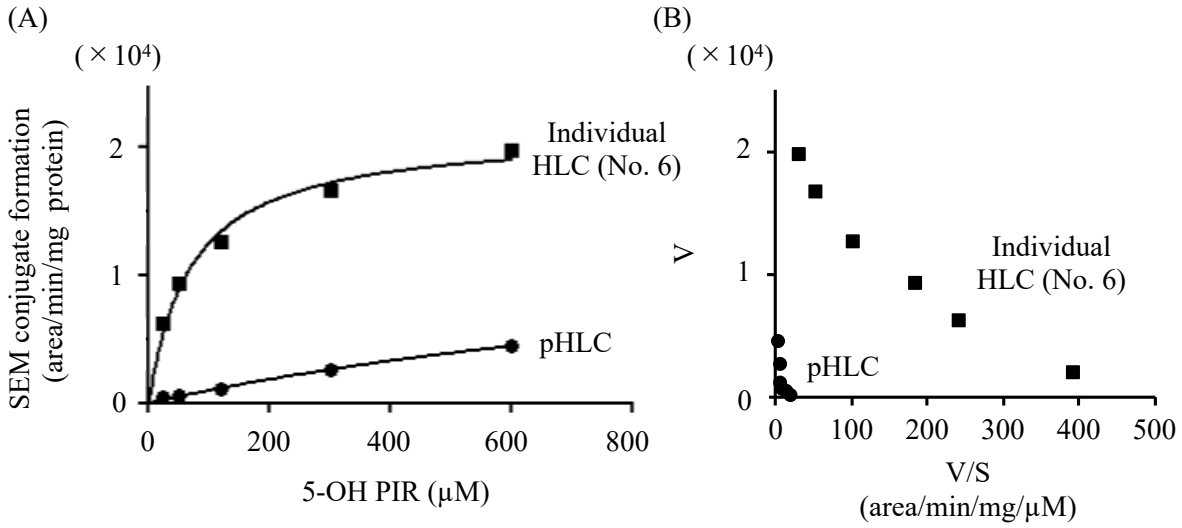

Supplemental Figure 2. The kinetics of SEM conjugate formation by individual HLC (No. 6) overlaid onto those by pHLC shown in Figure 5C. (A) S-V and (B) Eadie–Hofstee plots of the SEM conjugate formation from 5-OH PIR. 5-OH PIR at 5–600 μM was incubated with 0.5 mg/ml individual HLC in the presence of 20 μM disulfiram. Each point represents the mean ± SD of triplicate determinations.

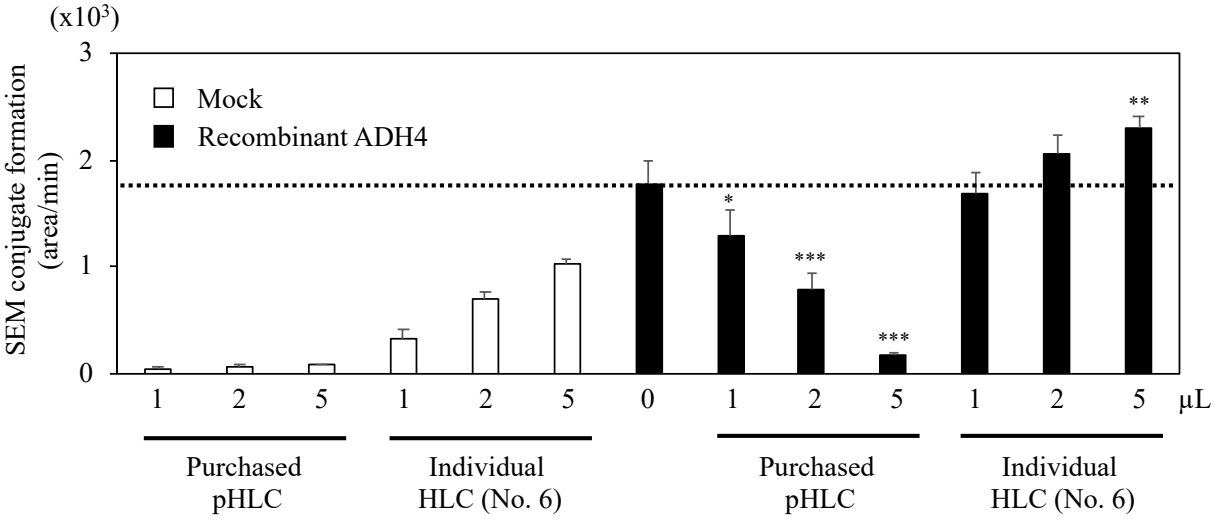

Supplemental Figure 3. The SEM conjugate formation by recombinant ADH4 in the presence of purchased pHLC or individual HLC (No. 6). Each column represents the mean ± SD of triplicate determinations. $^{*}P < 0.05$, $^{**}P < 0.01$, and $^{***}P < 0.001$, compared to SEM conjugate formation by recombinant ADH4 in the absence of HLC (ANOVA, Dunnett's test).